



JGR Solid Earth

RESEARCH ARTICLE

10.1029/2018JB016575

Key Points:

- Tsunami source for 2009 Dusky Sound, New Zealand, earthquake is determined using sparse deep water absolute pressure gauge and coastal tide gauge data
- Assimilation of tsunami data from dense array of seafloor differential pressure gauges is used in simulation of rapid forecast of 2009 Dusky Sound tsunami
- Improvement of tsunami forecast is found by merging forward computation from rapid earthquake W-phase model with tsunami data assimilation

Supporting Information:

- Supporting Information S1
- Movie S1
- Movie S2

Correspondence to:

A. F. Sheehan,
anne.sheehan@colorado.edu

Citation:

Sheehan, A. F., Gusman, A. R., & Satake, K. (2019). Improving forecast accuracy with tsunami data assimilation: The 2009 Dusky Sound, New Zealand, tsunami. *Journal of Geophysical Research: Solid Earth*, 124, 566–577. <https://doi.org/10.1029/2018JB016575>

Received 18 AUG 2018

Accepted 18 DEC 2018

Accepted article online 20 DEC 2018

Published online 10 JAN 2019

Improving Forecast Accuracy With Tsunami Data Assimilation: The 2009 Dusky Sound, New Zealand, Tsunami

Anne F. Sheehan¹ , Aditya R. Gusman² , and Kenji Satake³

¹Department of Geological Sciences and Cooperative Institute for Research in Environmental Sciences (CIRES), University of Colorado Boulder, Boulder, CO, USA, ²GNS Science, Lower Hutt, New Zealand, ³Earthquake Research Institute, University of Tokyo, Tokyo, Japan

Abstract We use tsunami waveforms recorded on deep water absolute pressure gauges (Deep-ocean Assessment and Reporting of Tsunamis), coastal tide gauges, and a temporary array of seafloor differential pressure gauges (DPG) to study the tsunami generated by the 15 July 2009 magnitude 7.8 Dusky Sound, New Zealand, earthquake. We first use tsunami waveform inversion applied to Deep-ocean Assessment and Reporting of Tsunamis seafloor pressure gauge and coastal tide gauge data to estimate the fault slip distribution of the Dusky Sound earthquake. This fault slip estimate is then used to generate synthetic tsunami waveforms at each of the DPG sites. DPG instruments are unfortunately not well calibrated, but comparison of the synthetic tsunami waveforms to those observed at each DPG site allows us to determine an appropriate amplitude scaling to apply. We next use progressive data assimilation of the amplitude-scaled DPG observations to retrospectively forecast the Dusky Sound tsunami wavefields and find a good match between forecast and observed tsunami wavefields at the Charleston tide gauge station on the west coast of New Zealand's South Island. While an advantage of the data assimilation method is that no initial condition is needed, we find that our forecast is improved by merging tsunami forward modeling from a rapid W-phase earthquake source solution with the data assimilation method.

Plain Language Summary Most tsunami warnings rely on first locating and determining size of a large earthquake and then using a computer model to estimate the size and timing of the resulting tsunami. Seafloor pressure gauges can also provide important data for studying tsunamis. Seafloor pressure increases as the peak of a tsunami wave passes overhead due to the increase in the height of the water column. In cases where a dense array of seafloor pressure gauges is available, a new “data assimilation” method can be applied to estimate the tsunami using the observations of pressure changes. In this paper we apply the data assimilation method to the tsunami generated from the 2009 Dusky Sound, New Zealand, magnitude 7.8 earthquake and determine a rapid and accurate estimate of the tsunami wave arrival time and size along the west coast of New Zealand. We next merge the two methods—first using a computer model to estimate the tsunami given information about the earthquake and then using seafloor pressure observations to refine the tsunami model—and find that the tsunami forecast accuracy is further improved. Studies such as this are important to test and further develop rapid and accurate tsunami warning systems.

1. Introduction

Existing tsunami forecasting systems usually utilize a combination of seismic and tsunami measurements. Global seismic networks provide enough data to accurately estimate the magnitude and hypocenter of an earthquake within minutes. A tsunami forecasting system that is equipped with precomputed tsunami propagation model may provide a rapid tsunami forecast from only earthquake magnitude and location information. However, these earthquake parameters may not be enough to give an accurate tsunami forecast when the earthquake is not a common event and cannot be represented by any of the scenarios in the precomputed database. Estimation of earthquake fault parameters from moment tensor solution is crucial for accurate tsunami forecasting. For rapid assessment of tsunami potential, W phases from broadband stations can be inverted to estimate an initial moment tensor solution (Gusman & Tanioka, 2014; Kanamori & Rivera, 2008; Tanioka et al., 2017). This solution can be then used in tsunami simulation to forecast coastal tsunami heights. Real-time coastal GNSS stations also can be used for rapid and accurate rupture quantification in real time (e.g., Crowell et al., 2012; Murray et al., 2018; Ohta et al., 2012).

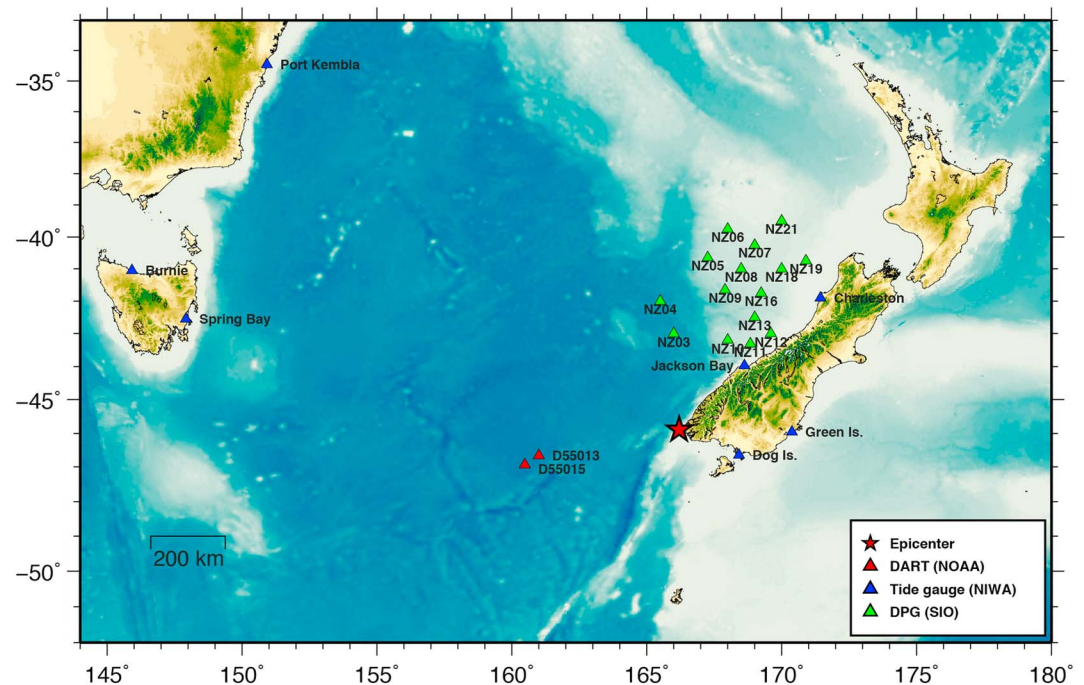


Figure 1. Map of the New Zealand region showing ocean bottom seismometers and differential pressure gauges of the MOANA experiment (green triangles), DART buoy tsunami seafloor pressure sensors (red triangles), and coastal tide gauge (blue triangles) stations used in this study. Red star represents the epicenter of the 2009 Dusky Sound earthquake. MOANA = Marine Observations of Anisotropy near Aotearoa; DART = Deep-ocean Assessment and Reporting of Tsunamis.

Data assimilation of offshore dense array pressure gauges is an alternative method that can be used for tsunami forecasting. Utilization of dense array data in data assimilation can give timely and accurate forecast even without any information about the tsunami source (e.g., location, mechanism, and magnitude). A tsunami data assimilation algorithm, which is based on the optimum linear interpolation method (Kalnay, 2003), was made by Maeda et al. (2015). This method can produce and refine an estimated tsunami wavefield around a tsunami dense array. The tsunami data assimilation method was tested using hypothetical scenarios and synthetic waveforms on the Japanese dense network of offshore pressure gauges off the east coast of Japan (S-Net). The method was further tested using real tsunami data observed by the Ocean Bottom Seismometer (OBS) network of the Cascadia Initiative in the Cascadia subduction zone (Gusman et al., 2016; Sheehan et al., 2015; Wang et al., 2017). This relatively new approach of tsunami data assimilation method needs more tests with different network configurations and different tectonic settings.

On 15 July 2009, a Mw 7.8 tsunamigenic earthquake occurred offshore the South Island of New Zealand, near Dusky Sound. According to the GeoNet New Zealand earthquake catalog, the hypocenter is located at 45.77025°S, 166.58707°E, 12 km depth, and occurred at 9:22:29 UTC. The focal mechanism of the earthquake from the Global Centroid Moment Tensor solution suggests an oblique thrust fault mechanism with seismic moment of 5.7×10^{20} Nm, strike of 25°, dip of 26°, and rake of 138°. The coseismic fault slip distribution of the earthquake has been estimated by inversion of global positioning system and differential interferometric synthetic aperture radar observations by Beavan et al. (2010). This previous study suggests that the earthquake ruptured a section in the Puysegur subduction interface with a dimension of 80 km by 50 km. The largest estimated slip amount was approximately 5 m, and the major slip region is located offshore. Prasetya et al. (2011) studied the size and extent of the generated tsunami in the earthquake source region, especially along the fiords of the Fiordland National Park in the southwest of New Zealand's South Island. Their model results give maximum tsunami elevations inside these long, narrow, and deep inlets between 0.5 and 2.0 m with maximum flow speeds up to 3.0 m/s. The earthquake also occurred during the 1-year deployment of the Marine Observations of Anisotropy near Aotearoa (MOANA) OBS network (Collins et al., 2009; Yang et al., 2012) (Figure 1). The 30-station MOANA network was equipped with

broadband ocean bottom seismometers and differential pressure gauges (DPG) sited offshore east and west of the South Island of New Zealand.

In this paper we use data assimilation both with and without a starting source model to simulate a forecast of the Dusky Sound tsunami. For the data assimilation we use Dusky Sound tsunami waveforms recorded on the array of seafloor DPGs of the MOANA ocean bottom seismic experiment (Collins & Molnar, 2014; Zietlow et al., 2014). We also perform a tsunami source inversion, by using tsunami waveforms from Deep-ocean Assessment and Reporting of Tsunamis (DART) stations (González et al., 1998) and tide gauges. The tsunami source inversion provides synthetic waveforms for calibrating the instrument response of the DPGs. The calibration process would not be practical to perform on a real-time basis, but once calibrated, DPG data could in principle be used in tsunami assimilations if the data are available in real time. Simulations using real data, such as those presented here, help demonstrate the utility of data assimilation using recordings on arrays of seafloor pressure gauges for tsunami warnings.

2. The 2009 Dusky Sound Tsunami Observations

Clear tsunami waveforms of the 2009 Dusky Sound earthquake were observed at two DART buoys (D55013 and D55015), four tide gauges in New Zealand (Charleston, Jackson Bay, Green Island, and Dog Island), three tide gauges in Australia (Port Kembla, Burnie, and Spring Bay), and on many of the seafloor pressure gauges of the MOANA deployment (Figure 1).

DART seafloor absolute pressure records for the Dusky Sound earthquake and tsunami were obtained from the National Oceanic and Atmospheric Administration—National Data Buoy Center (<http://www.ndbc.noaa.gov/dart.shtml>). The absolute pressure gauge, used by the DART and increasingly in other geophysical and oceanographic studies (Crawford et al., 2015; Phillips et al., 2008; Wallace et al., 2016), makes use of a quartz transducer with oscillation period related to stress, and thus to pressure (Houston & Paros, 1998). Coastal tide gauge records were obtained from the Intergovernmental Oceanographic Commission—United Nations Educational, Scientific and Cultural Organization sea level monitoring (<http://www.ioc-sea-levelmonitoring.org/index.php>) and the National Institute of Water and Atmospheric Research (<https://www.niwa.co.nz/>). The sampling interval of the tide gauge is 60 s, while that of the DART is 15–60 s (event mode vs. continuous). For waveform data processing and inversion purposes, we resampled the time series data to 15 s of time interval. To remove the ocean tides and high-frequency waves from the records in order to obtain the tsunami waveforms, the original records are band-pass filtered with cutoff periods of 100 min (0.000167 Hz) and 5 min (0.00333 Hz).

The MOANA OBS were deployed at water depths ranging from 550 to 4,700 m with average distance between stations of approximately 100 km. In addition to a three-component broadband seismometer, each OBS package had a Cox-Webb DPG (Cox et al., 1984; Webb et al., 1991). The DPG is a pressure gauge configured to respond to the difference between the ocean and the fluid in a reference chamber. The DPG was designed to detect pressure fluctuations in the frequency range from a few millihertz to a few hertz. The tsunami frequency band is outside of this frequency range, but the DPG roll-off toward the low frequency is gradual, which makes it possible to record tsunami signals (Sheehan et al., 2015). The 15 July 2009 Dusky Sound earthquake occurred very close to the MOANA network, the closest station (NZ01) was located only ~150 km away from the epicenter. Most of the MOANA DPGs recorded the tsunami of the Dusky Sound earthquake and only records from NZ15 and NZ17 were not available.

We retrieved MOANA DPG data starting 3 hr before the Dusky Sound earthquake origin time and ending 9 hr after for analysis. We then processed the records by removing trend, removing mean, decimating from the 50 sps recording to 1 sps, applying 5% Hanning taper, and band-pass filtering from 0.0002 to 0.005 Hz (200–5,000 s) using a Butterworth filter. The filtering helps with removing signals from outside the periods of interest, as well as reducing long-period noise, which is amplified in the deconvolution step. We tapered again, and then deconvolved the instrument response with frequency limits flat from 0.0003 to 0.005 Hz. Waveforms illustrating the processing steps are given in Figure S4 in the supporting information. The DPG instrument response is not well determined, and in order to reduce long-period artifacts and better recover the tsunami waveforms, we used a modified version of the IRIS-supplied instrument response (Table S2). The resulting response has one zero at (0,0), one pole at $(-1.2568e-03,0)$, and constant of $1.567662e+03$ Pa. The real part of the pole is reduced relative to the IRIS-provided value (Table S3), and

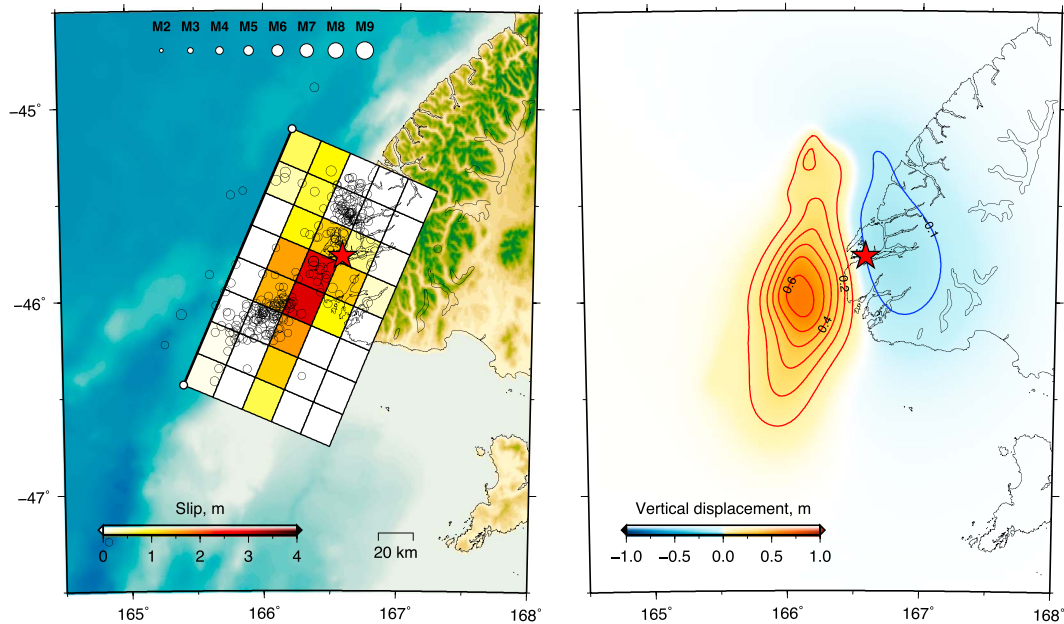


Figure 2. Slip distribution and the corresponding coseismic vertical displacement for Dusky Sound earthquake estimated by tsunami waveform inversion using DART and tide gauge data. Red star represents the epicenter of the earthquake. Dusky Sound aftershocks with magnitude >4 from GeoNet earthquake catalog (<http://quakesearch.geonet.org.nz>) from 15 to 30 July 2009 shown by open circles in left panel. DART = Deep-ocean Assessment and Reporting of Tsunamis.

the change in pole results in a change in amplitude and waveform shape (phase) of the processed DPG data, with resulting waveform shape in better agreement with synthetic tsunami waveforms and with fewer lower-frequency artifacts (Figure S4). The low-pass frequency of DPGs is dependent on the viscosity of the oil in the pressure gauge, which can be quite different between the laboratory and the seafloor, making them difficult to calibrate (Araki et al., 2005; Stahler et al., 2016). Example waveforms demonstrating the effect of each of the processing steps are shown in Figure S4.

The DPG data were clipped at several of the MOANA stations due to the large amplitude of the Dusky Sound seismic waves. In these cases, we hand-cut the DPG waveform data to eliminate clipped data prior to any processing. Clipping was particularly problematic at the DPG stations closest to the Dusky Sound earthquake (NZ01, NZ02, NZ03, and NZ04) and was present at 17 out of the 28 DPG stations. In the case of NZ01 and NZ02 the tsunami arrival was coincident with the clipped part of the waveform, and the tsunami signal could not be recovered. In the case of the other stations, the clipped part of the recording was prior to the tsunami arrival, and the tsunami part of the waveform was not affected. An example showing removal of clipped data is shown in Figure S4. Hand processing of clipped data is not practical in a real-time warning scenario; thus, instruments that can record bottom pressures on scale are important for real-time tsunami warning networks.

3. Fault Slip Distribution

For tsunami waveform inversion (Gusman et al., 2015; Satake, 1987), we arranged 8×5 subfaults with size of $20 \text{ km} \times 20 \text{ km}$ and the total fault length and width of 160 and 100 km (Figure 2). The dip of 25° and rake of 131° used for the subfaults are based on the U.S. Geological Survey (USGS) W-phase moment tensor solution. Instead of using the USGS W-phase strike angle of 26° , we use strike of 23.5° based on a previous study by Beavan et al. (2010), which makes our fault model geometry better aligned with the geometry of the plate interface and gives better waveform fits. The seafloor displacement for each subfault was calculated by the formula in Okada (1985). Tsunami waveform data at four tide gauges in New Zealand (Charleston, Jackson Bay, Green Is., and Dog Is.), two DART buoys offshore New Zealand (D55013 and D55015), and three tide gauges in Australia (Port Kembla, Burnie, and Spring Bay) were used in the inversion. To produce the Green's functions for the inversion, first, the tsunami waveforms were computed by solving the linear

shallow water equation in the spherical coordinate system (Gusman et al., 2010). Then the synthetic tsunami waveforms were corrected by a frequency-dependent phase correction method (Watada et al., 2014) to include the wave dispersion, the elastic loading, sea water compressibility, and gravitational potential change effects. The bathymetry data used for the tsunami simulation is based on the 30 arc-sec gridded bathymetry data of GEBCO (Weatherall et al., 2015). The grid size for the tsunami simulation at the New Zealand tide gauges and the DART buoys was 30 arc-sec, while that at the Australian tide gauges was 90 arc-sec. A tsunami waveform time interval of 15 s is chosen for the inversion. The slip amount of each sub-fault is estimated using a nonnegative least squares inversion (Lawson & Hanson, 1974).

The epicenter is located onshore and near the coast, but we find that the major slip region is located both onshore and offshore to the southwest of the epicenter. The fault slip distribution that we solve for has a large slip of 4 m (Figure 2a). The maximum slip occurs in the middle subfaults, in the depth interval 16–25 km. The maximum surface uplift is 0.7 m and the maximum subsidence is 0.1 m (Figure 2b). The main features of the slip distribution are consistent with the previous result by Beavan et al. (2010), but our model produces better fits to the observed tsunami waveforms (Figure 3a). This is not surprising because the slip distribution in our study is estimated using tsunami waveforms, while the previous study used crustal deformation data observed by differential interferometric synthetic aperture radar and global positioning system stations.

4. DPG Data Correction

We next compare the fit between the simulated tsunami waveforms from the modeled slip distribution with the observed tsunami waveforms on the processed MOANA DPGs (Figure 3c). We concentrate on the DPGs off the west coast of the South Island as they are less affected by refraction of the tsunami wave front around Stewart Island and are of greater interest to us for the tsunami assimilation study. We find that the simulated tsunami arrival time and waveform shape are consistent with the DPG observations but that the simulated amplitude is larger than that observed. A previous study using DPG data compared to absolute pressure gauge data from the Cascadia Initiative experiment has shown that amplitude scaling needs to be applied to DPG data for use in tsunami studies (Sheehan et al., 2015).

The observed and simulated peak amplitudes of the main tsunami pulse on the MOANA DPGs are compared in Figure 3b, and linear regression yields a correction factor of 3.3. However, there is significant scatter and several of the stations give observed waveforms which are still underfit after applying the correction. Given the scatter, the tsunami waveform at each station is corrected by the ratio between the observed and simulated peak amplitude at the station. The data set for tsunami assimilation consists of amplitude corrected observations for the 16 DPGs off the west coast with good data, plus simulated tsunami waveforms for the stations, which had poor or no data (clipped at NZ01 and NZ02, no data at NZ15 and NZ17, low-frequency artifacts at station NZ14).

5. Tsunami Data Assimilation

We use a data assimilation method with MOANA DPG observations for a retrospective simulation of forecast for the Dusky Sound tsunami. In the tsunami data assimilation method (Maeda et al., 2015), at every time step the tsunami wavefield for the current time step is approximated by numerically solving the shallow water equations using the wavefield at the previous time step (i.e., by a forward numerical simulation). In the assimilation step, the forecasted tsunami height is compared to that observed at the DPG stations, and this residual is used as a correction to bring the assimilated wavefield closer to the true wavefield. We use a smoothing matrix with cutoff distance of 10 km from the station to transmit the information of tsunami amplitude from the station to the surrounding area. With the tsunami data assimilation process, \mathbf{x} is a matrix of the computed wavefield with three components (amplitude, flow velocity in $-x$ and $-y$ directions) on the modeling grid. We start with an estimated tsunami wavefield at the $(n - 1)$ th time step, \mathbf{x}_{n-1}^a , and obtain the wavefield at the next time step by $\mathbf{x}_n^f = \mathbf{F}\mathbf{x}_{n-1}^a$, where \mathbf{F} represents the tsunami forward modeling equations, \mathbf{x}^a is the assimilated wavefield, and \mathbf{x}^f is the forecasted wavefield (Maeda et al., 2015). In the case of data assimilation with no initial condition, the \mathbf{x}_{n-1}^a at the beginning of the simulation (\mathbf{x}_0^a) is zero. In the first iteration, $\mathbf{x}_1^f = \mathbf{F}\mathbf{x}_0^a$. After this we loop through time and at each time step calculate the assimilated wavefield

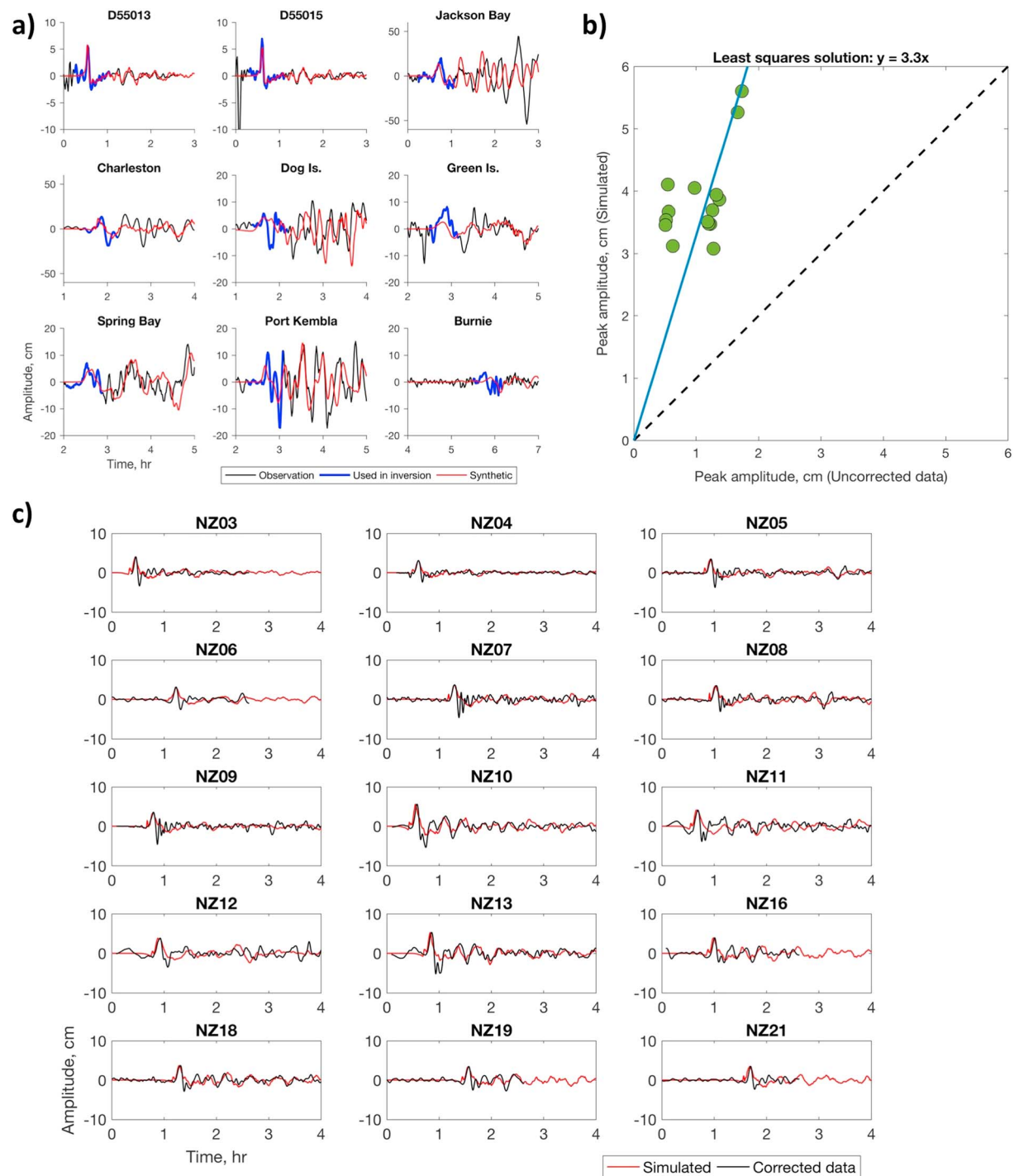


Figure 3. (a) DART and tide gauge tsunami waveforms used in inversion for slip distribution. Observed (black) and simulated (red). Blue lines represent the parts of the observed waveforms used in the tsunami waveform inversion. (b) Comparison between peak amplitudes of simulated and observed tsunami waveforms at the MOANA DPG stations. (c) Comparison between amplitude-corrected observed (black) and simulated (red) tsunami waveforms at the MOANA-DPG stations. The simulated MOANA DPG waveforms are obtained using the slip distribution obtained using DART and tide gauge data. MOANA = Marine Observations of Anisotropy near Aotearoa; DART = Deep-ocean Assessment and Reporting of Tsunamis; DPG = differential pressure gauges.

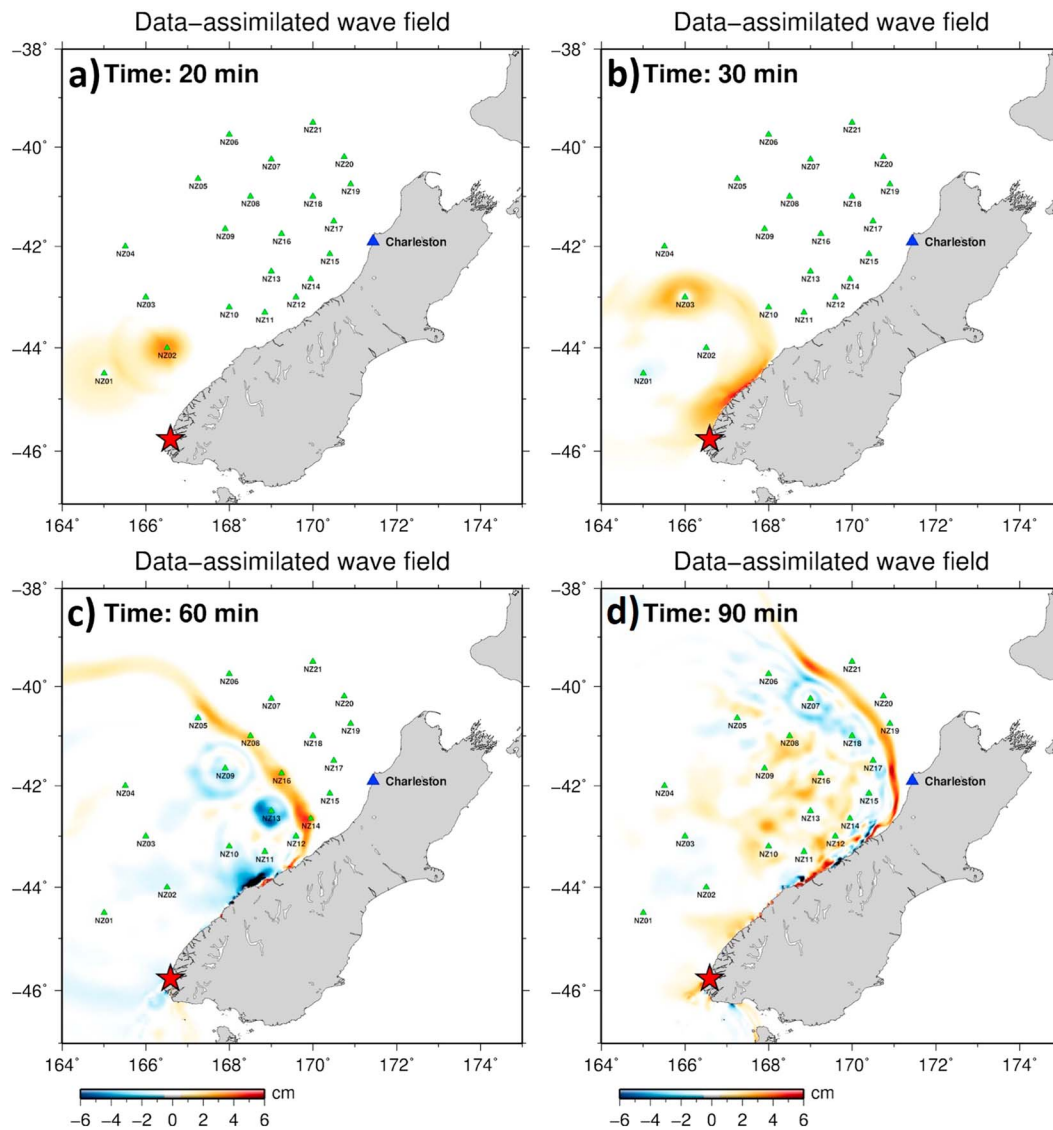


Figure 4. Dusky Sound tsunami wavefield estimated by tsunami data assimilation of MOANA DPG data with zero initial condition. Dusky Sound epicenter is denoted by red star. Wavefield scale in centimeters. Snapshots of data assimilated tsunami wavefields at (a) 20, (b) 30, (c) 60, and (d) 90 min are shown. MOANA DPG stations used in the data assimilation (green triangles). MOANA = Marine Observations of Anisotropy near Aotearoa; DPG = differential pressure gauges.

$\mathbf{x}_n^a = \mathbf{x}_n^f + \mathbf{W}[\mathbf{y}_n - \mathbf{H}\mathbf{x}_n^f]$ (equation 2 of Maeda et al., 2015), where \mathbf{y}_n is the observed tsunami amplitude at the stations, \mathbf{W} is a weighting matrix, and \mathbf{H} is an operator to access the simulated amplitude at the stations from the whole simulated wavefield \mathbf{x}_n^f . In the case of data assimilation with initial condition, which we introduce in this paper, the \mathbf{x}_{n-1}^a at the beginning of the simulation is the initial vertical displacement calculated using the fault model parameters. The vertical displacement is the amplitude component of matrix \mathbf{x} , and the initial flow velocities in -x and -y directions are zero. The data assimilation with initial condition is in a sense a hybrid method of tsunami data assimilation and forward modeling based on seismic data analysis. The initial tsunami wavefield is computed from initial condition based on W-phase analysis, but it will be corrected using the information of the observed tsunami waveforms.

5.1. Forecasting Without Initial Model

An advantage of the data assimilation method is that it does not require an initial source and in principle could run continuously to rapidly and automatically forecast a tsunami as the initial waves are observed

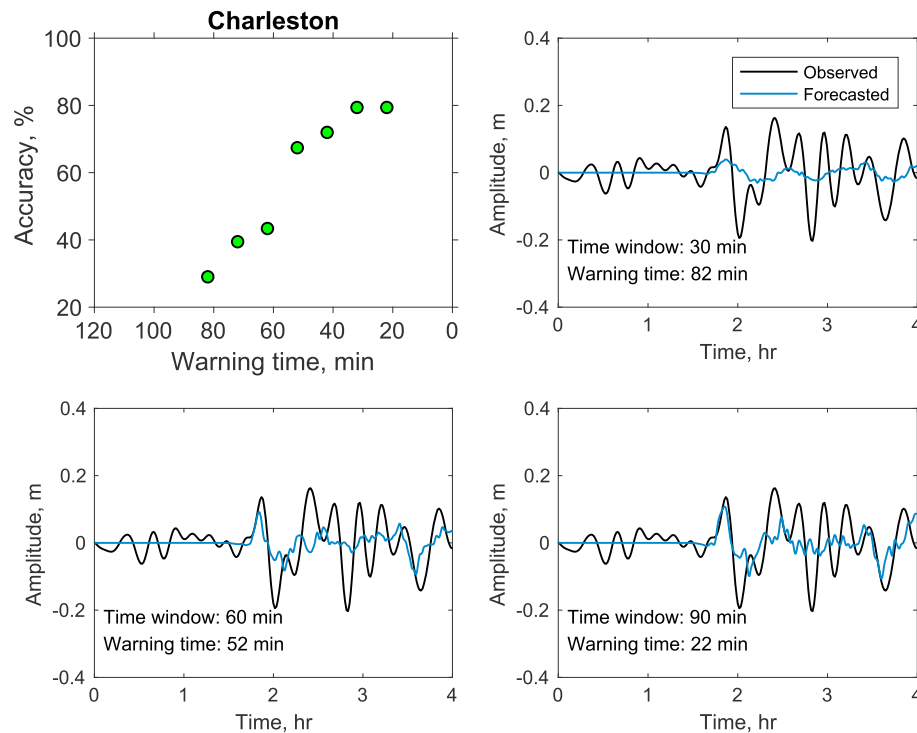


Figure 5. Dusky Sound tsunami forecast accuracy at Charleston, New Zealand, tide gauge station from the tsunami data assimilation method with zero initial condition. The waveform comparisons are from results of tsunami data assimilation using 30, 60, and 90 min of data at the MOANA DPG stations, starting at the earthquake origin time. Warning time is the time difference between tsunami data assimilation and tsunami arrival time at Charleston. Accuracy is from equation (2). MOANA = Marine Observations of Anisotropy near Aotearoa; DPG = differential pressure gauges.

at an array of seafloor pressure gauges. The computation domain for our tsunami data assimilation includes a geographical area from 38° to 47°S and from 164° to 175°W, with a grid spacing of 1 km. We resample our DPG data to 1-s sampling rate as the data assimilation is run with a 1-s time step. Our results for the Dusky Sound tsunami using data assimilation with no initial source model are shown in Figures 4 and 5. The initial tsunami wavefield arrives at station NZ02 approximately 20 min after the earthquake's origin time (Figure 4a). Since no tsunami source is assumed in this data assimilation, we do not expect accurate wavefields at the beginning of the data assimilation process. After the tsunami passes through several stations, a more realistic wavefield emerges (Figures 4b–4d). This tsunami wavefield (amplitude and velocity) from the tsunami data assimilation method is then used in numerical forward modeling to forecast the tsunami at tide gauges. The simulated tsunami wavefields at every 10 min from 30 min after the Dusky Sound earthquake until 90 min after the earthquake are used to forecast the tsunami at the Charleston tide gauge station on the northwest coast of the South Island of New Zealand (Figure 5). The tsunami first peak arrival at Charleston is 112 min after the earthquake, this arrival time minus the time window used in the tsunami data assimilation is used to calculate the warning time.

The accuracy of the forecast is quantified by calculating the geometric mean ratio (K) of the observed (O) and simulated (S) first peak tsunami amplitudes at the Charleston tide gauge station following the method of Aida (1978). The geometric mean ratio (equation (1)) can be converted into percent accuracy using equation (2).

$$\log(K) = \frac{1}{N} \sum_{i=1}^N \log\left(\frac{O_i}{S_i}\right) \quad (1)$$

$$\text{Accuracy}(\%) = \begin{cases} \frac{1}{K} \times 100, & K \geq 1 \\ K \times 100, & K < 1 \end{cases} \quad (2)$$

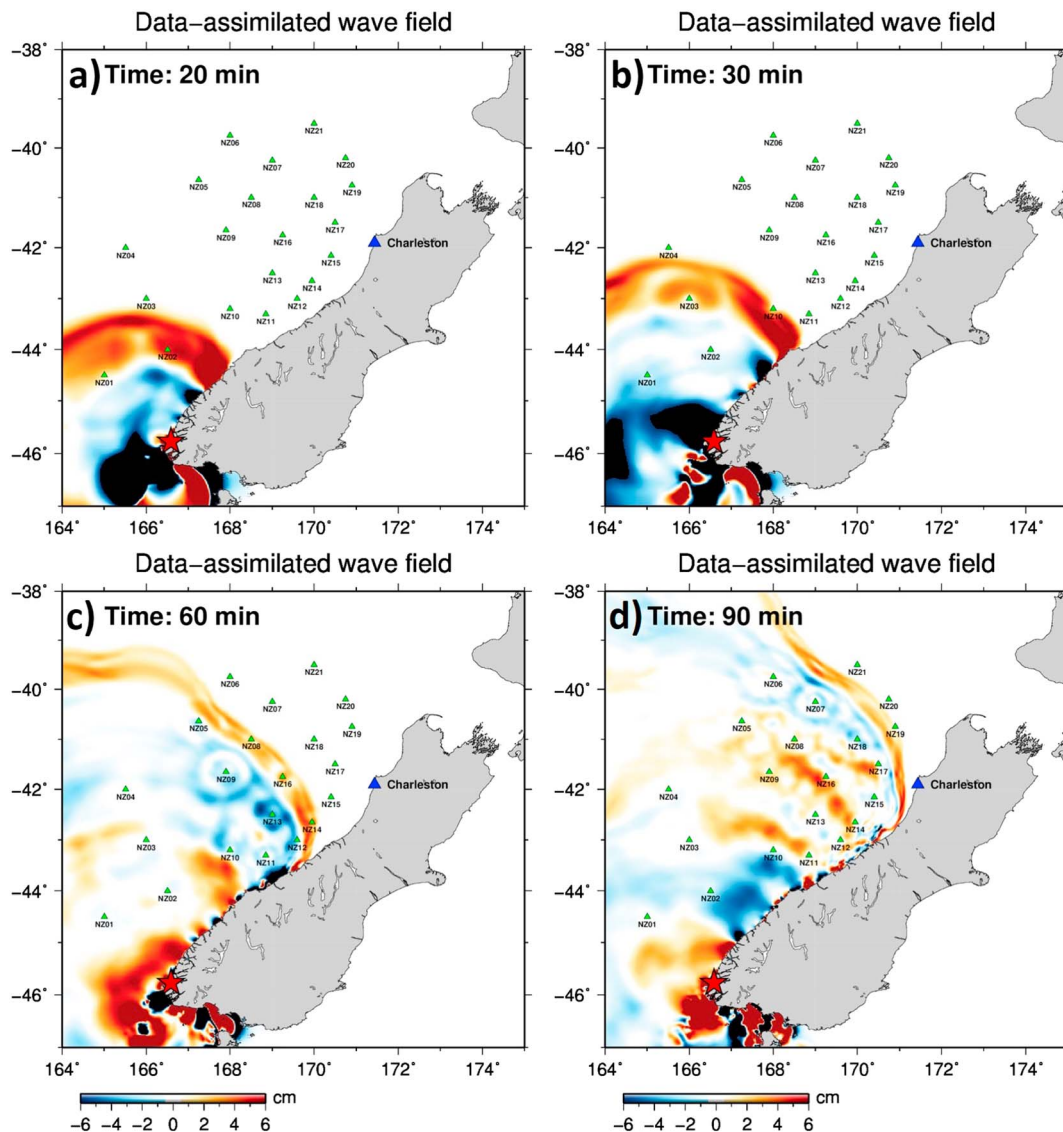


Figure 6. Dusky Sound tsunami wavefield estimated by tsunami data assimilation of MOANA DPG observations using W-phase solution as initial condition. Snapshots of data assimilated tsunami wavefields at (a) 20, (b) 30, (c) 60, and (d) 90 min are shown. MOANA DPG stations used in the data assimilation (green triangles). MOANA = Marine Observations of Anisotropy near Aotearoa; DPG = differential pressure gauges.

where N is the number of observations, which is 1 in this case. The simulation result is better if the corresponding K value is closer to 1. When K value is larger than 1, it indicates that the model underestimates the observation. Conversely, when K value is smaller than 1, it indicates that the model overestimates the observation.

The accuracy improves as a longer time series is used in the assimilation, but this trades off with a shorter warning time (Figure 5). For example, the data assimilation using 30 min of data underpredicts the tsunami amplitude at Charleston (30% accuracy) but gives 82 min of warning time, whereas the data assimilation using 90 min of data has an accuracy of 80% but warning time of only 22 min at Charleston.

5.2. Forecasting With Initial Simple Fault Model

We next explore the use of a rapidly determined initial fault model as an initial condition to improve the accuracy of the data assimilation forecast. We use the W-phase inversion algorithm (Duputel et al., 2011; Kanamori & Rivera, 2008) to obtain the focal mechanism of the 2009 Dusky Sound earthquake. W-phase

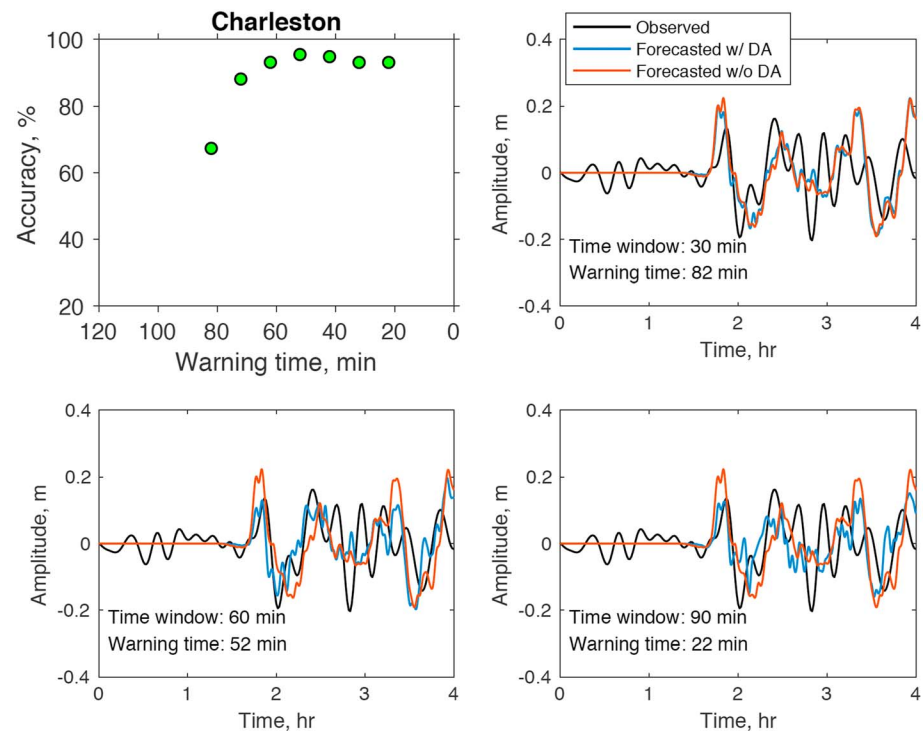


Figure 7. Tsunami forecast accuracy at Charleston, New Zealand, tide gauge station from the tsunami data assimilation (DA) method using W-phase solution as initial condition. The waveform comparisons are from results of tsunami data assimilation using 30, 60, and 90 min of data at the MOANA DPG stations, starting at the earthquake origin time. Accuracy is from equation (2). Warning time is the time difference between tsunami data assimilation and tsunami arrival time at Charleston. Solution using W-phase solution without data assimilation shown in red for comparison, note that the W-phase without DA forecast waveform does not change with time, whereas the version with DA does.

waveforms recorded within 7 min after the earthquake (stations within 14° epicentral distance) are used (Figure S5). Our solution has a moment magnitude of 7.9, which is slightly higher than the Global Centroid Moment Tensor and final USGS W-phase solutions, fault plane of strike 353° , dip 15° , and rake 79° , and auxiliary plane with strike 184° , dip 75° , and rake 93° (Figure S6). Of the two nodal planes, the fault plane is chosen because it best aligns with the subduction zone geometry and expected orientation of a megathrust earthquake. Simulations exploring the use of the auxiliary plane rather than the fault plan are provided in Figures S1–S3. The point here is to obtain an extremely rapid source solution to use as an initial condition for the data assimilation, so it is not surprising that there are some differences between the rapid solution and those obtained with more time and more data. We make a single fault model from the 7 min W-phase inversion result. The fault length and width are calculated from the estimated moment magnitude using the scaling relation of Blaser et al. (2010). The vertical displacement is calculated using the Okada half space model (Okada, 1985). This vertical displacement is then used as the initial condition for the tsunami data assimilation algorithm.

We first use the initial vertical displacement of the W-phase solution in forward tsunami modeling. The forward modeling allows us to get a rapid tsunami forecast even before the tsunami waveforms in the array are used in the data assimilation. The modeled amplitude is overestimated at Charleston, which is not unexpected since the rapid W-phase solution magnitude is high relative to the final solution. The W-phase forward modeled forecast has an accuracy of 63% at Charleston.

The simulated wavefield from the W-phase solution is then used as an initial condition in the data assimilation process. Our results of tsunami data assimilation using the W-phase initial condition are shown in Figures 6 and 7. Since an initial condition is used, the data-assimilated wavefield at the early time steps looks reasonable even before observations are available from any of the MOANA DPG stations (Figure 6a). This is

because at time steps before the tsunami arrives at the MOANA DPG stations, the wavefield is the W-phase forward model. At later time steps the incoming tsunami observations at the MOANA DPG stations are used to correct the assimilated wavefield (Figures 6b–6d). The tsunami forecast accuracy at the Charleston tide gauge station from the data assimilation with W-phase initial condition has a 65% accuracy at 30 min after the earthquake origin time, providing 82 min of warning at Charleston, in comparison to only 30% accuracy for the data assimilation with no initial condition. The model produced at 60 min has accuracy of over 90% and provides 52 min of warning (Figure 7).

6. Conclusions

We used seafloor pressure data from a portable deployment of ocean bottom seismometers to retrospectively forecast the 2009 Dusky Sound tsunami offshore the South Island of New Zealand. The amplitudes of the DPG waveforms were first corrected using simulated tsunami waveforms generated using a source model that we obtained from inverting DART and tide gauge data. The corrected tsunami waveforms were then used in a data assimilation scheme to provide a tsunami forecast along the west coast of New Zealand. We introduced the use of data assimilation of observed tsunami waveforms to correct the tsunami wavefield computed from a rapidly determined W-phase earthquake source solution. While a significant advantage of forward computation from W-phase source solution is rapid forecast, we found that the addition of data assimilation can improve the accuracy of the resulting tsunami forecast.

Acknowledgments

We thank Rob Bell from NIWA for assistance with New Zealand tide gauge data and George Mungov from NOAA NCEI for DART data. The ocean bottom pressure data used were from the MOANA experiment led by John Collins, using OBS from the Scripps Institutional Instrument Contributor of the U.S. National Ocean Bottom Seismic Instrumentation Pool (www.obsip.org). We thank John Collins, John Orcutt, Glen Sasagawa, Spahr Webb, and Wayne Crawford for information and discussion about DPG instrument responses. We thank Takuto Maeda for making his tsunami data assimilation code available. Many of the figures were made using the public domain generic mapping tools (Wessel & Smith, 1998). This work was initiated while A. F. S. was a visiting professor at the Earthquake Research Institute (ERI), University of Tokyo. Support for this research came in part from NSF EAR 0409835, the CIRES Innovative Research Program, and public research funding from the Government of New Zealand. Seafloor pressure data used in this study are available from the National Oceanic and Atmospheric Administration—National Data Buoy Center (<http://www.ndbc.noaa.gov/dart.shtml>) for DART data and from the Incorporated Research Institutions for Seismology Data Management Center (<http://ds.iris.edu>) for MOANA DPG data (network ZU 2009–2010). Tide gauge records are available from the Intergovernmental Oceanographic Commission—United Nations Educational, Scientific and Cultural Organization sea level monitoring (<http://www.ioc-sealevelmonitoring.org/index.php>) and the National Institute of Water and Atmospheric Research (<https://www.niwa.co.nz/>). The authors state that they do not have any real or perceived financial conflicts of interest related to this work.

References

- Aida, I. (1978). Reliability of a tsunami source model derived from fault parameters. *Journal of Physics of the Earth*, 26(1), 57–73. <https://doi.org/10.4294/jpe1952.26.57>
- Araki, E., Sugioka, H., & Shiobara, H. (2005). A deep sea differential pressure gauge. *Frontier Research on Earth Evolution*, 2, 1–5.
- Beavan, J., Samsonov, S., Denys, P., Sutherland, R., Palmer, N., & Denham, M. (2010). Oblique slip on the Puysegur subduction interface in the 2009 July MW 7.8 Dusky Sound earthquake from GPS and InSAR observations: Implications for the tectonics of southwestern New Zealand. *Geophysical Journal International*, 183(3), 1265–1286. <https://doi.org/10.1111/j.1365-246X.2010.04798.x>
- Blaser, L., Kruger, F., Ohrnberger, M., & Scherbaum, F. (2010). Scaling relations of earthquake source parameter estimates with special focus on subduction environment. *Bulletin of the Seismological Society of America*, 100(6), 2914–2926. <https://doi.org/10.1785/0120100111>
- Collins, J., Sheehan, A., Molnar, P. (2009). Marine Observations of Anisotropy near Aotearoa, International Federation of Digital Seismograph Networks, Other/Seismic Network. https://doi.org/10.7914/SN/ZU_2009
- Collins, J. A., & Molnar, P. (2014). Pn anisotropy beneath the South Island of New Zealand and implications for distributed deformation in continental lithosphere. *Journal of Geophysical Research: Solid Earth*, 119, 7745–7767. <https://doi.org/10.1002/2014JB011233>
- Cox, C., Deaton, T., & Webb, S. (1984). A deep-sea differential pressure gauge. *Journal of Atmospheric and Oceanic Technology*, 1(3), 237–246. [https://doi.org/10.1175/1520-0426\(1984\)001<0237:ADSDPG>2.0.CO;2](https://doi.org/10.1175/1520-0426(1984)001<0237:ADSDPG>2.0.CO;2)
- Crawford, W., Ballu, V., Bertin, X., & Karpytchev, M. (2015). The sources of deep ocean infragravity waves observed in the North Atlantic Ocean. *Journal of Geophysical Research: Oceans*, 120, 5120–5133. <https://doi.org/10.1002/2014JC010657>
- Crowell, B. W., Bock, Y., & Melgar, D. (2012). Real-time inversion of GPS data for finite fault modeling and rapid hazard assessment. *Geophysical Research Letters*, 39, L09305. <https://doi.org/10.1029/2012GL051318>
- Duputel, Z., Rivera, L., Kanamori, H., & Hayes, G. (2011). Real-time W phase inversion during the 2011 off the Pacific coast of Tohoku earthquake. *Earth, Planets and Space*, 63(7), 535–539. <https://doi.org/10.5047/eps.2011.05.032>
- González, F. I., Milburn, H. M., Bernard, E. N., & J. C. Newman (1998). Deep-ocean Assessment and Reporting of Tsunamis (DART): Brief overview and status report. Paper presented at Proceedings of the International Workshop on Tsunami Disaster Mitigation, Tokyo, Japan, 19–22 January 1998.
- Gusman, A. R., Murotani, S., Satake, K., Heidarzadeh, M., Gunawan, E., Watada, S., & Schurr, B. (2015). Fault slip distribution of the 2014 Iquique, Chile, earthquake estimated from ocean-wide tsunami waveforms and GPS data. *Geophysical Research Letters*, 42, 1053–1060. <https://doi.org/10.1002/2014GL062604>
- Gusman, A. R., Sheehan, A. F., Satake, K., Heidarzadeh, M., Mulia, I. E., & Maeda, T. (2016). Tsunami data assimilation of Cascadia seafloor pressure gauge records from the 2012 Haida Gwaii earthquake. *Geophysical Research Letters*, 43, 4189–4196. <https://doi.org/10.1002/2016GL068368>
- Gusman, A. R., & Tanioka, Y. (2014). W phase inversion and tsunami inundation modeling for tsunami early warning: Case study for the 2011 Tohoku event. *Pure and Applied Geophysics*, 171(7), 1409–1422. <https://doi.org/10.1007/s00024-013-0680-z>
- Gusman, A. R., Tanioka, Y., Kobayashi, T., Latief, H., & Pandoe, W. (2010). Slip distribution of the 2007 Bengkulu earthquake inferred from tsunami waveforms and InSAR data. *Journal of Geophysical Research*, 115, B12316. <https://doi.org/10.1029/2010JB007565>
- Houston, M. H., & Paros, J. M. (1998). High accuracy pressure instrumentation for underwater applications. In *Proc. 1998 Int. Symp. Underwater Technol.* (pp. 307–311). Tokyo, Japan: IEEE. <https://doi.org/10.1109/UT.1998.670113>
- Kalnay, E. (2003). *Atmospheric modeling, data assimilation, and predictability*. Cambridge: Cambridge University Press.
- Kanamori, H., & Rivera, L. (2008). Source inversion of W phase: Speeding up seismic tsunami warning. *Geophysical Journal International*, 175(1), 222–238. <https://doi.org/10.1111/j.1365-246X.2008.03887.x>
- Lawson, C. L., & Hanson, R. J. (1974). *Solving least squares problems*. Englewood Cliffs: Prentice-Hall.
- Maeda, T., Obara, K., Shinohara, M., Kanazawa, T., & Uehira, K. (2015). Successive estimation of a tsunami wavefield without earthquake source data: A data assimilation approach toward real-time tsunami forecasting. *Geophysical Research Letters*, 42, 7923–7932. <https://doi.org/10.1002/2015GL065588>

- Murray, J. R., Crowell, B. W., Grapenthin, R., Hodgkinson, K., Langbein, J. O., Melbourne, T., et al. (2018). Development of a geodetic component for the U.S. West Coast earthquake early warning system. *Seismological Research Letters*, *89*(6), 2322–2336. <https://doi.org/10.1785/0220180162>
- Ohta, Y., Kobayashi, T., Tsushima, H., Miura, S., Hino, R., Takasu, T., et al. (2012). Quasi real-time fault model estimation for near-field tsunami forecasting based on RTK-GPS analysis: Application to the 2011 Tohoku-Oki earthquake (Mw 9.0). *Journal of Geophysical Research*, *117*, B02311. <https://doi.org/10.1029/2011JB008750>
- Okada, Y. (1985). Surface deformation due to shear and tensile faults in a half-space. *Bulletin of the Seismological Society of America*, *75*(4), 1135–1154.
- Phillips, K. A., Chadwell, C. D., & Hildebrand, J. A. (2008). Vertical deformation measurements on the submerged south flank of Kilauea volcano, Hawai'i reveal seafloor motion associated with volcanic collapse. *Journal of Geophysical Research*, *113*, B05106. <https://doi.org/10.1029/2007JB005124>
- Prasetya, G., Beavan, J., Wang, X., Reyners, M., Power, W., Wilson, K., & Lukovic, B. (2011). Evaluation of the 15 July 2009 Fiordland, New Zealand tsunami in the source region. *Pure and Applied Geophysics*, *168*(11), 1973–1987. <https://doi.org/10.1007/s00024-011-0282-6>
- Satake, K. (1987). Inversion of tsunami waveforms for the estimation of a fault heterogeneity: Method and numerical experiments. *Journal of Physics of the Earth*, *35*(3), 241–254. <https://doi.org/10.4294/jpe1952.35.241>
- Sheehan, A. F., Gusman, A. R., Heidarzadeh, M., & Satake, K. (2015). Array observations of the 2012 Haida Gwaii tsunami using Cascadia Initiative absolute and differential seafloor pressure gauges. *Seismological Research Letters*, *86*(5), 1278–1286. <https://doi.org/10.1785/0220150108>
- Stahler, S. C., Sigloch, K., Hosseini, K., Crawford, W. C., Barruol, G., Schmidt-Aursch, M. C., et al. (2016). Performance report of the RHUM-RUM Ocean Bottom Seismometer network around La Reunion, western Indian Ocean. *Advances in Geosciences*, *41*, 43–63.
- Tanioka, Y., Miranda, G. J. A., Gusman, A. R., & Fujii, Y. (2017). Method to determine appropriate source models of large earthquakes including tsunami earthquakes for tsunami early warning in Central America. *Pure and Applied Geophysics*, *174*(8), 3237–3248. <https://doi.org/10.1007/s00024-017-1630-y>
- Wallace, L. M., Webb, S. C., Ito, Y., Mochizuki, K., Hino, R., Henrys, S., et al. (2016). Slow slip near the trench at the Hikurangi subduction zone, New Zealand. *Science*, *352*(6286), 701–704. <https://doi.org/10.1126/science.aaf2349>
- Wang, Y., Satake, K., Maeda, T., & Gusman, A. R. (2017). Green's function-based tsunami data assimilation: A fast data assimilation approach toward tsunami early warning. *Geophysical Research Letters*, *44*, 10,282–10,289. <https://doi.org/10.1002/2017GL075307>
- Watada, S., Kusumoto, S., & Satake, K. (2014). Traveltime delay and initial phase reversal of distant tsunamis coupled with the self-gravitating elastic Earth. *Journal of Geophysical Research: Solid Earth*, *119*, 4287–4310. <https://doi.org/10.1002/2013JB010841>
- Weatherall, P., Marks, K. M., Jakobsson, M., Schmitt, T., Tani, S., Arndt, J. E., et al. (2015). A new digital bathymetric model of the world's oceans. *Earth and Space Science*, *2*, 331–345. <https://doi.org/10.1002/2015EA000107>
- Webb, S. C., Zhang, X., & Crawford, W. (1991). Infragravity waves in the deep ocean. *Journal of Geophysical Research*, *96*(C2), 2723–2736. <https://doi.org/10.1029/90JC02212>
- Wessel, P., & Smith, W. H. F. (1998). New, improved version of generic mapping tools released. *Eos, Transactions American Geophysical Union*, *79*(47), 579. <https://doi.org/10.1029/98EO00426>
- Yang, Z., Sheehan, A. F., Collins, J. A., & Laske, G. (2012). The character of seafloor ambient noise recorded offshore New Zealand: Results from the MOANA ocean bottom seismic experiment. *Geochemistry, Geophysics, Geosystems*, *13*, Q10011. <https://doi.org/10.1029/2012GC004201>
- Zietlow, D. W., Sheehan, A. F., Molnar, P. H., Savage, M. K., Hirth, G., Collins, J. A., & Hager, B. H. (2014). Upper mantle seismic anisotropy at a strike-slip boundary: South Island, New Zealand. *Journal of Geophysical Research: Solid Earth*, *119*, 1020–1040. <https://doi.org/10.1002/2013JB010676>